Scaling for Saturated Moist Quasi-Geostrophic Turbulence

Marguerite L. Brown[a] , Olivier Pauluis[a] , Edwin P. Gerber[a]

[a] *Center for Atmosphere Ocean Science, Courant Institute, New York, New York*

Corresponding author: Marguerite Brown, mlb542@nyu.edu

ABSTRACT: Much of our conceptual understanding of midlatitude atmospheric motion comes from two-layer quasi-geostrophic (QG) models. Traditionally, these quasi-geostrophic models don't include moisture, which accounts for an estimated 30-60% of the available energy of the atmosphere. The atmospheric moisture content is expected to increase under global warming, and therefore a theory for how moisture modifies atmospheric dynamics is crucial. We use a two-layer moist quasi-geostrophic model with convective adjustment (MQG) as a basis for analyzing how latent heat release and large-scale moisture gradients impact the scalings of a midlatitude system at the synoptic scale. In this model, the degree of saturation can be tuned independently of other moist parameters by enforcing a high rate of evaporation from the surface. This allows for study of the effects of latent heat release at saturation, without the intrinsic nonlinearity of precipitation. At saturation, this system is equivalent to the dry QG model under a rescaling of both length and time. This predicts that the most unstable mode shifts to smaller scales, the growth rates increase, and the inverse cascade extends to larger scales. We verify these results numerically, and use them to verify a framework for the complete energetics of a moist system.

SIGNIFICANCE STATEMENT: The effect of moist processes, especially the impact of latent heating associated with condensation, on the size and strength of mid-latitude storms is not well understood. Such insight is particularly needed in the context of global warming, as we expect moisture to play a more important role in a warmer world. In this study, we provide intuition into how including condensation can result in mid-latitude storms that grow faster and have features on both larger and smaller scales than their dry counterparts. We provide a framework for quantifying these changes and verify it for the special case where it is raining everywhere. These findings can be extended to the more realistic situation where it is only raining locally.

1. Introduction

A major challenge to our understanding of midlatitude storm systems lies in the interplay between the atmospheric circulation and the hydrological cycle. On a global scale, higher temperature and humidity in the tropics relative to the poles drives poleward transport of both sensible and latent heat. On the local scale, ascending parcels undergo adiabatic expansion, condensing excess moisture and releasing latent heat. This additional energy can induce local hydrodynamical instabilities in conditions that would otherwise be stable. The effect of moisture is not isolated to the scales on which condensation occurs, but rather impacts dynamics across a broad range of scales, including the aggregate behavior of storm tracks (Shaw et al. 2016), the extratropical stratification (Frierson et al. 2006; Schneider and O'Gorman 2008; Wu and Pauluis 2014), and the global atmospheric circulation (Pauluis et al. 2010). Understanding the impacts of moist processes across the full range of geophysical scales is necessary to understand how midlatitude storm dynamics will change in a world becoming more humid as a result of climate change.

The two-layer quasigeostrophic model is one of simplest mathematical models to exhibit the basic features of the turbulent midlatitude atmosphere, from planetary scale barotropic jets to synoptic scale baroclinic eddies that organize into storm tracks. Its relative simplicity, coupled with its ability to capture key dynamical features, has made it a good choice for studying the broader statistical and scaling properties of a dry atmosphere, e.g. Vallis (2006). While its utility in assessing the moist case is limited on account of the tendency for real-world moist systems to have large deviations in effective static stability, a two-layer quasigeostrophic model including moisture and precipitation provides insight into changes in criticality, scaling, and other properties of turbulence without confounding influences from the tropics. The goal of this study is to use the moist two-layer quasi-geostrophic model (MQG) of Lapeyre and Held (2004) to bring intuition from the classic dry model to a moist atmosphere. The concepts verified in this idealized system establish hypotheses worth testing with more complex simulations and reanalysis data.

Where, then, do we expect moisture to have an effect on midlatitude dynamics? Both global and local-scale effects have been identified, relating to latent heat as a source of potential energy in the atmosphere. On a global scale, moisture has a meridional gradient corresponding to that of temperature, such that the tropics have a much higher moisture content than the poles. Latent heat contained within moist air accounts for between 30-60% of the available energy of a moist atmosphere (Lorenz 1978). A more complete picture of the meridional energy profile that acts as a reference state of the system can be obtained by studying the meridional gradient of thermodynamic quantities that include both temperature and moisture. This is critical for understanding the response of the midlatitude atmosphere to global warming, where we expect the moisture gradient to undergo a larger change than the temperature gradient due to the non-linear dependence of moisture content on temperature.

As a thought experiment, how do we expect global warming to impact the midlatitude circulation? As demonstrated by Atmospheric Model Intercomparison Project (AMIP) experiments, the first order impact of global warming can be captured by uniformly warming the surface of an atmospheric model, a 2 or 4 K warming roughly approximating the impact of a doubling or quadrupling of CO2, respectively. Naively, the temperature gradient is unaffected, but the moisture gradient will increase by approximately 7% per Kelvin, assuming relative humidity remains fixed. Translating these changes to our conceptual two-layer quasi-geostrophic model is challenging.

Locally, condensation in ascending parcels releases latent heat, which partially compensates for the adiabatic expansion associated with pressure and density differences within the atmosphere. Following our thought experiment, this reduction in effective static stability has lead to the concept of gross moist static stability (Emanuel et al. 1994), which in the simple dry quasigeostrophic framework, would have to be accounted for in the background stratification. Convection also translates the meridional moisture gradient at the surface to a meridional temperature gradient in the upper troposphere. One could modify the large scale forcing of the quasi-geostrophic model to capture this change in temperature, but in the process we have uncoupled the two effects of moisture on vertical and meridional gradients.

Additionally, latent heat release, through enhanced convection, leads to systems with a faster growth rate and smaller-scale storms (Emanuel et al. 1987). The preferential lower-level convergence and upper-level divergence associated with latent heat release generates positive (cyclonic) potential vorticity in the lower atmosphere and negative (anticyclonic) potential vorticity in the upper atmosphere, causing moist systems to have an asymmetry in cyclone/anticyclone generation not found in dry ones (Emanuel et al. 1987; Lapeyre and Held 2004).

Characterizing the changes to scales and growth rates associated with moist processes requires an energetic framework that accounts for the additional energy generated by latent heat release. Ideally, this framework would be formulated in a way that can be readily interpreted from both intuitive and mathematical perspectives, allowing for application to different moist models and a clear delineation of energy sources and sinks. Understanding the physical intuition behind a moist formulation of energy and potential vorticity can help bridge the gap between different mathematical formulations of the moist energy budget. Conceptualizations of moist energetics draw on the notion that both dry and moist effects relax the atmosphere towards a reference state - baroclinic adjustment to a meridional temperature gradient for the dry dynamics and precipitation relaxation to a moisture profile for the moist dynamics - to construct a notion of a statistical equilibrium reference state characterized by some combination of dry and moist dynamics (Emanuel et al. 1994). Examples of mathematical formulations of the energetics include the framework of Lapeyre and Held (2004), based on the moist static stability and moisture deficit of the system, and of Smith and Stechmann (2017), with Heavyside functions distinguishing saturated regions from unsaturated.

Previous studies (Emanuel et al. 1987; Lambaerts et al. 2011a,b, 2012; Lapeyre and Held 2004) have explored changes in the scale of instability associated with moisture. Stronger moist effects typically leads to smaller scale motions and narrower regions of saturation. This correlation obfuscates the effect of different mechanisms by which moisture induces smaller scale motion. For instance, does the shift arise as a result of highly localized precipitation? Would a similar result persist even if the precipitation characteristically occurred on larger scales? And how do different mechanisms combine under the non-linearity of precipitation and Clausius-Clayperon? Edwards et al. (2019) explored some spectral scalings in the saturated limit, but without a trigger for latent heat release, such as convective adjustment.

We use the model of Lapeyre and Held (2004) as a basis for exploring the scaling questions involved in assessing a moist turbulent system. This model has the advantages of having a convective trigger for the onset of precipitation and allowing for a system which can become supersaturated. In this study, we will restrict ourselves to the fully saturated case to take advantage of the linearity of the system under this constraint, with the understanding that a clear next step would be to utilize information about both the dry and fully saturated limits to explore the scalings of partially saturated systems. In the saturated case, we will demonstrate that the inclusion of moisture results in a broadening of the turbulent spectrum: the high wave-number cutoff shifts to smaller scales, growth rates increase across all scales, and the Rhines scale, associated with the termination of the inverse cascade, shifts to larger scales.

The model is described in Section 2. Section 3 illustrates the changes to criticality and instability associated with the saturated limit and how those are expected to impact the injection scales of instability. Section 4 presents the spectral features of the inertial range and the energetic framework for understanding moist dynamics, and we conclude our study in Section 5.

2. Model Description

The model used in this paper matches the two-layer moist quasigeostrophic (MQG) model described in Lapeyre and Held (2004), depicted in Figure 1. The MQG model consists of two layers of equal mean depth H in a doubly periodic domain. Rotational dynamics are captured by a β plane in which the Coriolis parameter is expressed linearly in the meridional coordinate as $f = f_0 + \beta y$. The system is stratified, such that each layer has a characteristic potential temperature θ_i with $\theta_1 - \theta_2 = \delta\theta > 0$.

a. The Dry System

The classic 2-layer quasi-geostrophic (QG) system has been explored in depth, as in e.g. Vallis (2006). The geostrophic dynamics of such a system can be decomposed into a barotropic streamfunction $\psi_B = (\psi_1 + \psi_2)/2$, the column-integrated "bulk" movement of the system, and the baroclinic streamfunction $\psi_b = (\psi_1 - \psi_2)/2$, the vertical gradient of the system. The corresponding

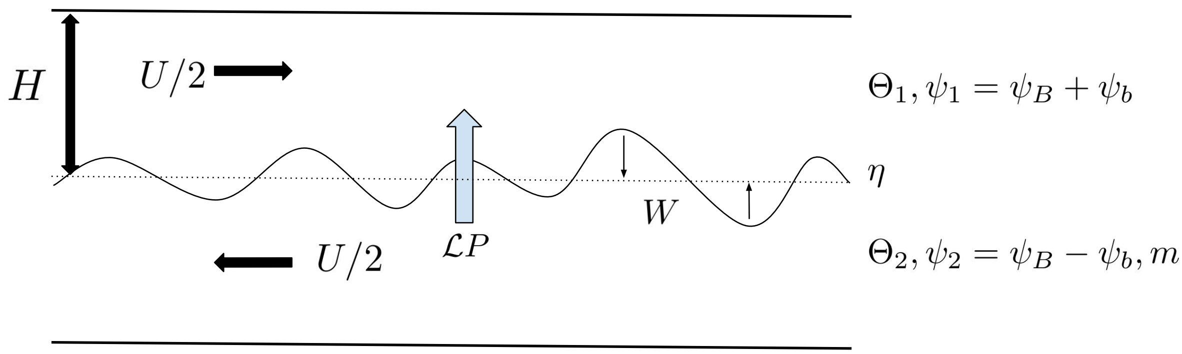

FIG. 1. Structure of the two-layer model. Thick flat lines correspond to surfaces that remain fixed and the wavy curve to the interface η, which varies. Each layer has a streamfunction relating to the barotropic and baroclinic modes as described in the text, an associated potential temperature, and a typical height scale H. The interface η captures variations from this typical thickness, which are corrected by vertical motion W. The moisture m is confined to the lower layer and precipitation conditionally triggers mass transport $\mathcal{L}P$ from the bottom to the top layer. Ekman dissipation $r\nabla^2(\psi_B - \psi_b)$ takes effect at the bottom surface.

geostrophic velocities are given by $(u_i, v_i) = \left(-\partial_y\psi_i, \partial_x\psi_i\right)$ in mode $i = B, b$, and the corresponding vorticities $\zeta_i = \nabla^2\psi_i$. The vorticities evolve as,

$$\frac{D_B}{Dt}(\zeta_B + \beta y) = -J(\psi_b, \zeta_b) - \frac{r}{2}(\zeta_B - \zeta_b) \tag{1}$$

$$\frac{D_B}{Dt}\zeta_b = -J(\psi_b, \zeta_B + \beta y) - f_0\frac{W}{H} + \frac{r}{2}(\zeta_B - \zeta_b). \tag{2}$$

Here, the $J(\cdot,\cdot)$ indicates the Jacobian and $D_B/Dt = \partial_t + J(\psi_B, \cdot)$ indicates the material derivative with respect to the barotropic flow. Both the barotropic and baroclinic vorticities are advected by the large-scale barotropic flow and forced by nonlinear interactions between the two modes characterized by the first term of the right hand side. Baroclinic vorticity is additionally generated when the ageostrophic convergence W/H transports mass between the two layers. The mass is transported upward (downward) when W/H is positive (negative), corresponding with a generation of anticyclonic (cyclonic) baroclinic vorticity. Finally, Ekman damping at the bottom surface dissipates both barotropic and baroclinic vorticity at large scales and introduces additional interchanges between the two modes. Additional external forcings may be included in both equations, but are here neglected for simplicity.

The interface η between the two layers evolves with both the vertical and horizontal transport of mass. This interface acts as a proxy for temperature, and we will interchangeably refer to the variable η by both descriptors in this paper. This interface then relates to the baroclinic mode via thermal wind balance

$$\eta = \frac{2H}{\lambda^2 f_0}\psi_b, \tag{3}$$

where $\lambda = \sqrt{g^* H}/f_0$ is the Rossby deformation radius, and $g^* = g\delta\theta/\theta_0$. The interface then evolves as

$$\frac{D_B}{Dt}\eta = -W + S, \tag{4}$$

where S indicates the total diabatic forcing, including both radiative cooling and latent heat release.

Equations (2) and (4) can be combined to eliminate the ageostrophic divergence term. This leads to the concept of potential vorticity (PV), defined for the barotropic mode as $q_B = \zeta_B + \beta y$; and for the baroclinic mode as $q_b = \zeta_b - f_0\eta/H$. Each have a corresponding mean background gradient $\overline{q}_B = \beta y$ and $\overline{q}_b = U\lambda^{-2}y$. The potential vorticities evolve as

$$\frac{D_B}{Dt}q_B = -J(\psi_b, q_b) - \frac{r}{2}(\zeta_B - \zeta_b) \tag{5}$$

$$\frac{D_B}{Dt}q_b = -J(\psi_b, q_B) + \frac{r}{2}(\zeta_B - \zeta_b) - f_0\frac{S}{H}. \tag{6}$$

The classic 2-layer QG model has $S = 0$. In this case, Equations (5) and (6) are a closed set of equations for two quantities which, in absence of dissipation, are conserved in the domain average. The inclusion of diabatic forcing terms disrupts this conservation.

b. Incorporating Moisture

Incorporating the effect of moisture in the two-layer QG model requires the inclusion of latent heat release in the diabatic forcing term S. In turn, this requires an equation for the water content. We assume that water is only present in the lower layer, and that the mixing ratio there is close to a reference value m_0. We then introduce a *thickness equivalent* mixing ratio m - with units of height - such that the total mixing ratio is $m_0(1 + m/H)$. Since the lower atmosphere contains the bulk of the moisture content, this weighted mixing ratio is defined only in the bottom layer of the system. It is continuously replenished by evaporation of water from the surface at rate E, which we will assume to be constant over the entire system. The water budget can then be written as

$$\frac{D_B}{Dt}m = J\left(\psi_b, m\right) + W - P + E. \tag{7}$$

Hence the water content is transported by the lower-level flow (here decomposed into barotropic and baroclinic components), removed by precipitation P, and replenished by surface evaporation E.

Water vapor condenses and releases latent heat when the value of m exceeds a saturation value m_s set by the Clausius-Clayperon relation, here represented by a linearization with respect to temperature η

$$m_s = C\eta = 2C\frac{\lambda^{-2}H}{f_0}\psi_b, \tag{8}$$

with C the gradient of Clausius-Clayperon with respect to temperature. At points where the mixing ratio exceeds this value - that is, where the system becomes supersaturated - the precipitation acts to relax the mixing ratio down to the saturation value with characteristic time τ, such that

$$P = \begin{cases} \left(m - m_s\right)/\tau = \left(m - C\eta\right)/\tau & \text{where } m > m_s \\ 0 & \text{where } m \leq m_s \end{cases}. \tag{9}$$

The diabatic forcing in Equation (4) consists of the combined effects of latent heat release and radiative cooling. Following the formulation of Lapeyre and Held (2004), we will set the choose the radiative cooling to be a fixed constant proportional to the evaporation E, such that the total diabatic forcing is given by

$$S \equiv \mathcal{L}\left(P - E\right), \tag{10}$$

with

$$\mathcal{L} \equiv \frac{Lm_0}{c_p\delta\theta} \in [0,1). \tag{11}$$

Here, L is the latent heat of vaporization, m_0 the reference mixing ratio, and $c_P\delta\theta$ characterizes the typical dry stability of the system. This non-dimensional term can be thought of as the typical ratio of the amount of available latent heat to the amount of sensible heat lost adiabatically by an ascending parcel. In the limit $\mathcal{L} \to 1$, the available latent heat can fully compensate for the adiabatic cooling of a parcel as it ascends, thereby contradicting the assumption of stratification.

c. *Moist Potential Vorticity*

The inclusion of latent heat release disrupts the conservation of the baroclinic PV. The question arises of whether we can construct a physically meaningful conserved quantity that serves a similar role to that of the dry baroclinic PV. The 'potential' part of PV indicates a reservoir which can be converted into vorticity. In the dry case, vertical motions W' draw from a reservoir of thickness anomalies η', removing them while generating baroclinic vorticity ζ_b:

$$\partial_t \eta' = -W'$$
$$\partial \zeta_b' = -f_0 \frac{W'}{H}.$$

In the QG system, the ratio of the change in interface thickness and vorticity is constant and equal to f_0/H. The potential vorticity can be thought of as the vorticity of the layer after its thickness perturbation is brought back to 0, so that the thickness perturbation to the (dry) potential vorticity is $-f_0\eta/H$.

In the moist case, the thickness evolution equation now includes a contribution from precipitation:

$$\partial_t \eta' = -W' + \mathcal{L}P'.$$

The contribution from precipitation partially compensates for the impacts of vertical motion. Hence the vertical motion may be better characterized by an effective thickness $\eta + \mathcal{L}m$, whose evolution equation, constructed from Equations (4) and (7), does not depend on precipitation:

$$\frac{D_B}{Dt}(\eta + \mathcal{L}m) = J(\psi_b, \mathcal{L}m) - (1-\mathcal{L})W. \tag{12}$$

By analogy with the dry model, the quantity $\eta + \mathcal{L}m$ can be thought of as a reservoir of baroclinic vorticity that can be converted through vertical motion. In the moist framework, this reservoir is enhanced through a combination of two effects: first, it includes a contribution from the moisture field in addition to the thickness perturbation, and, second, the impacts of vertical velocity is reduced by a factor $1-\mathcal{L} < 1$. Moist baroclinic potential vorticity, in concept, is then the baroclinic vorticity after the perturbation to the *effective thickness* $\eta + \mathcal{L}m$ is brought back to zero by vertical motion. This yields a *moist baroclinic potential vorticity* of the form

$$q_m = \zeta_b - \frac{1}{1-\mathcal{L}} \frac{f_0}{H} (\eta + \mathcal{L} m), \tag{13}$$

which is a baroclinic formulation based on the moist potential vorticity derived in Lapeyre and Held (2004). Its evolution equation is given by

$$\frac{D_B}{Dt} q_m = -J\left(\psi_b, q_B + \frac{f_0}{H} \frac{\mathcal{L} m}{1-\mathcal{L}}\right) + \frac{r}{2} (\zeta_B - \zeta_b). \tag{14}$$

d. Saturated Limit

The nonlinear "if" statement of the condensation trigger (9) introduces a major complication in the study of how moisture impacts dynamics. However, in the special case where the system is everywhere precipitating - in other words, where the "if" statement is replaced with a global "yes" - this nonlinearity is removed. This saturated case serves as a natural point of comparison with the dry case, in which the "if" statement is replaced with a global "no."

A second simplification arises if one makes the assumption that precipitation acts quickly enough to maintain the system near saturation. Within the quasi-geostrophic system described above, the limit of complete saturation can be nearly achieved by increasing the evaporation parameter E and decreasing the precipitation relaxation scale τ. The first increases the amount of water vapor added to the system at every time step, ensuring at sufficiently high values that the system is never sub-saturated. The latter decreases the amount of time that the system takes to relax to the saturated value, decreasing the value of the moisture surplus $m - m_s$ in a supersaturated system. Applying both of these limits corresponds to the Strict Quasi Equilibrium approximation of Emanuel et al. (1994).

From a mathematical point of view, the saturated limit amounts to enforcing the condition that the moisture is equal to its saturation value, i.e. $m = m_s = C\eta$. As a result, the moist PV can be written as

$$q_{ms} = \zeta_b - \mu_s \lambda^{-2} \psi_b. \tag{15}$$

This is similar to the expression for the baroclinic potential vorticity, but with the deformation radius rescaled by a factor $\mu_s^{-1/2}$, defined by

$$\mu_s = \frac{1+C\mathcal{L}}{1-\mathcal{L}} \geq 1. \tag{16}$$

This quantity characterizes the reduction in gross static stability associated with moist parameters, as in Emanuel et al. (1994), and will be discussed in greater detail in Section 4. Furthermore, the moist PV equation (14) becomes equivalent to the (dry) baroclinic PV equations, without precipitation and with a rescaled deformation radius.

$$\frac{D_B}{Dt} q_{ms} = -J\left(\psi_b, q_B\right) + \frac{r}{2}\left(\zeta_B - \zeta_b\right). \tag{17}$$

This saturated limit will be the focus of the scaling arguments for the remainder of the paper.

e. Numerical Setup

The real atmosphere has a meridional temperature forcing associated with incoming solar radiation. To capture the effect of this, we prescribe a linear background gradient (denoted with overbars) and model the evolution of the perturbation, denoted with a prime. The baroclinic streamfunction is prescribed a mean background gradient $\overline{\psi_b} = -U/2y$, associated with an externally forced temperature gradient. The total baroclinic streamfunction is $\psi_b = \overline{\psi_b} + \psi_b'$, with the prime denoting a perturbation. Since the baroclinic streamfunction has a background gradient, the interface also has a reference state $\overline{\eta} = -UHy/\lambda^2 f_0$. Correspondingly, the barotropic and baroclinic PV have mean gradients $\overline{Q}_B = \beta y$ and $\overline{Q}_b = Uy/\lambda^2$. In the dry case, instability occurs when the mean baroclinic PV gradient is larger than the gradient of the Coriolis parameter. This can be recast in terms of the criticality ξ as

$$\xi = \frac{U}{\beta\lambda^2} > 1. \tag{18}$$

The mixing ratio also has a meridional gradient associated with the temperature gradient, with higher moisture content near the equator than the poles. The moisture content preferentially adjusts towards the saturation value associated with the local temperature, with precipitation relaxing supersaturated regions towards the saturation value and while evaporation increases the moisture

Parameter	Expression	Realistic	Represents	Simulation Values
ξ	$\frac{U}{\beta\lambda^2}$	1	Dry Criticality	0.8, 1.0, 1.25
$\mathcal{R}$	$\frac{r\lambda}{U}$	.16	Ekman damping	.16
$\mathcal{L}$	$\frac{Lm_0}{c_p\delta\Theta}$	0.2-0.35	Moist Stability	0.0, 0.1, 0.2, 0.3, 0.4, 0.5, 0.6, 0.7
$\mathcal{C}$	C	2	Clausius-Clayperon effects	0.0, 2.0
$\mathcal{E}$	$\frac{Ef_0\lambda^2}{U^2m_0}$	0.4	Moisture Uptake	1000
τ^*	$\frac{\tau U}{\lambda}$	$< .15 - .85$	Precipitation timescale	0.0025
dt	$\frac{\Delta t U}{\lambda}$	N/A	Timestep	0.0005
ν^*	$U\lambda^7\nu$	N/A	Small scale dissipation	10^{-7}

TABLE 1. Tunable parameter space (nondimensionalized), realistic values, and the values used in the simulations here.

content globally. The reference state of the mixing ratio can then be set according by combining Equation (8) with the reference state of the temperature, yielding the background gradient $\overline{m} = C\overline{\eta} = -CUH/\lambda^2 f_0 y$. The moist baroclinic PV then has background gradient $\overline{q}_m = \mu_s U\lambda^{-2}y$.

Lastly, the implementation of precipitation requires a closure to account for strict non-negativity. We follow the closure of Lapeyre and Held (2004), described in Appendix A.

We perform experiments on a doubly periodic domain in spectral space with a 256x256 grid, The domain size is chosen such that $2\pi\lambda = L/9$. The simulations were run for a time $T = 400\lambda/U$. Time averages are computed over the last quarter of the run with sampling at intervals of $\delta t = .25\lambda/U$. Timestepping uses a 3rd order Adams-Bashforth method with an integrating factor to remove the stiff portion of the equation and with the Jacobian handled pseudo-spectrally with anti-aliasing. Timestepping is done for the upper, lower, and moist lower potential vorticity, thereby eliminating the need to compute the vertical motion W.

The simulations used for data in this paper span the ranges listed in the right column of Table 1. An additional run with $\xi = 5.0$, $\mathcal{L} = 0.0$, and $C = 0.0$ was used for comparison in Figure 2. Realistic values are listed in column 3 of Table 1. The estimate for the precipitation relaxation timescale τ^* comes from estimates for such in the tropics, which range from 2hrs (Betts and Miller 1986) to 12hrs (Bretherton et al. 2004). The rationale for all other physical parameters can be found in Lapeyre and Held (2004). The timestep was chosen based on the stability of the simulation over the desired time range. The higher order viscosity ν^* was chosen to allow for the dissipation of spurious numerical oscillations without suppressing the smaller-scale instability associated with latent heat release.

3. Linear Stability Analysis in the Saturated Limit

In many studies, the fully saturated case is equivalent to the dry case under some rescaling. Appendix B demonstrates that the same is true here, using the moist baroclinic potential vorticity instead of the dry and introducing modifications to characteristic length and time scales. We will here explore this rescaling in a linear stability analysis.

We recall that, in the dry case, instability occurs when the mean baroclinic potential vorticity gradient is larger than the gradient of the Coriolis parameter. Similarly, in the saturated limit, instability occurs when the *mean moist baroclinic potential vorticity gradient* is larger than the gradient of the Coriolis parameter, or, expressed in terms of a saturated criticality ξ_s

$$\xi_s \equiv \frac{\mu_s U}{\beta \lambda^2} \equiv \mu_s \xi > 1, \tag{19}$$

where ξ is the dry criticality.

We observe that μ_s is always larger than 1, which implies that the moist potential vorticity gradient is always larger than the baroclinic potential vorticity gradient, and thus that the saturated criticality ξ_s is higher than the dry criticality ξ. In particular, it is possible for the saturated system to be unstable with $\xi_s > 1$, even though the classical dry theory would predict stability (i.e. $\xi < 1$).

Figure 2 demonstrates that the scalings of moist systems cannot be determined by ξ or ξ_s alone. The top and middle rows depict the potential vorticities of a dry and moist simulation with the same value of ξ, demonstrating the increase in energy at both small and large scales associated with the inclusion of moisture. The middle and bottom rows depict the potential vorticities of a moist and dry simulation with the same value of ξ_s, demonstrating that the moist system exhibits smaller-scale vortices than the dry.

Figure 3 shows the growth rate as function of both the wave number modulus K and $\lambda_s = \mu_s^{-1/2}\lambda$, given by

$$\sigma = \frac{Uk}{(\lambda_s K)^4 + 2(\lambda_s K)^2}\left[\frac{(\lambda_s K)^8}{4} - (\lambda_s K)^4 + \xi_s^{-2}\right]^{1/2}, \tag{20}$$

where k is the wavenumber corresponding to propagation in the x (zonal) direction. Figure 3 considers the case with $K = k$. As with previous equations in the saturated linear instability analysis, Equation (20) matches the expression for the classic two-layer baroclinic instability, with

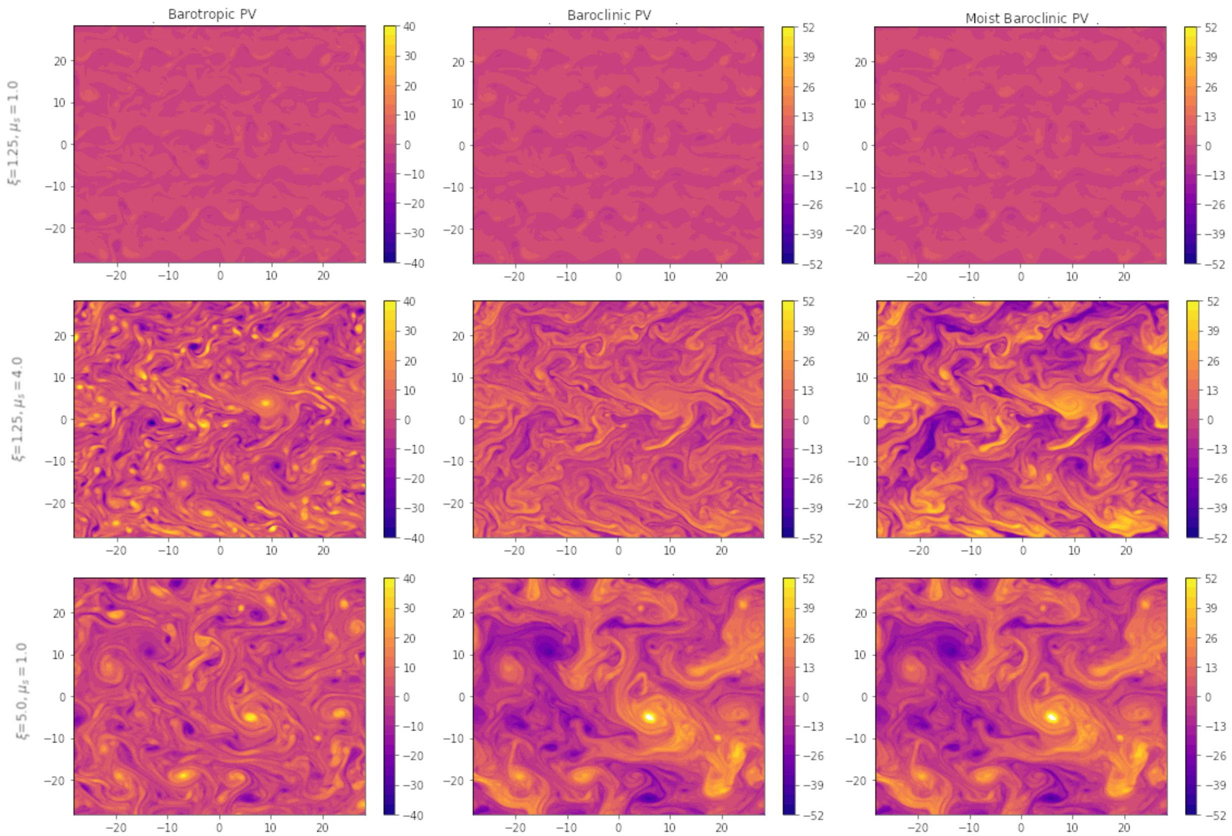

FIG. 2. Snapshots of the barotropic, baroclinic, and moist baroclinic potential vorticity perturbation for 3 cases. The top is a dry case with mild supercriticality. The second is a saturated case with the same dry criticality as the first, but with moist effects implemented. The third is another dry case with higher criticality. The second and third cases have same total saturated criticality. Both increases in criticality result in more energetic flows. The moist case has markedly higher small-scale vorticity, consistent with the shift to smaller scales described in the linear stability analysis. Furthermore, the middle row, as the only moist system, exhibits a smaller magnitude of dry baroclinic PV compared to the moist. This is associated with the inclusion of moisture in the 'reservoir' for conversion into baroclinic vorticity.

the saturated versions of criticality and the moist Rossby deformation radius replacing their dry counterparts.

The saturated limit also implies changes in the spectrum of unstable modes, which are confined between lower and upper wavenumber moduli K_- and K_+, defined by

$$K_\pm^4 = 2\mu_s^2\lambda^{-4}\left(1 \pm \sqrt{1-\mu_s^{-2}\xi^{-2}}\right). \tag{21}$$

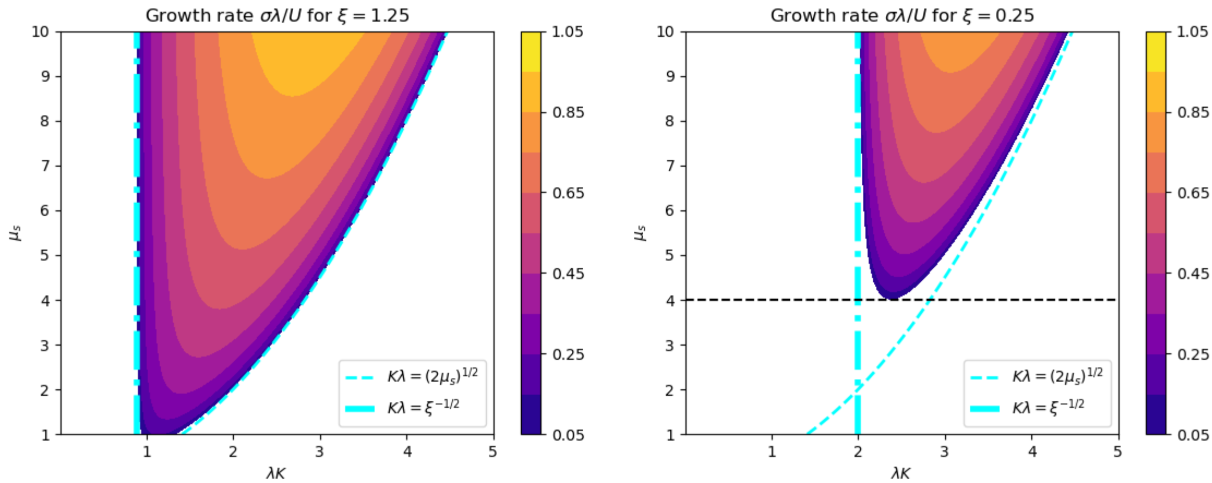

FIG. 3. Growth rate as a function of $K\lambda = |k|\lambda$ and μ_s, with ξ fixed as the value indicated in each title. The dashed horizontal line on the right corresponds to the value of μ_s necessary to achieve marginal saturated criticality. The two lines enveloping the contour correspond to asymptotic bounds on the unstable region, in the limit $\xi_s \longrightarrow \infty$.

The impact of the moist parameter μ_s is two-fold: the spectrum tends toward higher wave number, and the range of unstable modes also increases.

It is convenient to consider the limit of strong supercriticality ($\xi_s >> 1$), in which case the long and short wave cut off can be written as Equation (21)

$$K_{-}\lambda \approx \xi^{-1/2} \tag{22}$$

$$K_{+}\lambda \approx 2^{1/2}\mu_s^{1/2}. \tag{23}$$

Figure 3 demonstrates these asymptotic limits. While the short wave cutoff K_+ shifts to smaller scales as moist parameter μ_s increases, the long wave cut-off K_- exhibits little dependency on μ_s. It also indicates a broadening of the spectrum of unstable modes with increasing μ_s. Equation (20) is equivalent to the growth rate of the dry system, except with a rescaling of length according to to the moist Rossby deformation radius. We can therefore predict a shift in unstable modes as $\mu_s^{1/2}$ when ξ_s is held constant. Likewise, we may estimate that the fastest growth rate will increase similarly with $\mu_s^{1/2}$.

We can return to Figure 2 for intuition about how well these predictions play out. The middle and bottom rows have equal values of ξ_s. However, the middle row has $\mu_s = 4.0$, while the bottom row is dry. The results of the linear stability analysis predict that the middle row will have instability on a length scale that is a factor $\mu_s^{-1/2} = 0.5$ smaller than the typical length scale of the bottom row. Visually, this should mean that an enlarged snapshot of a quarter of the domain in the middle row resembles the corresponding PV in the bottom row.

4. Energetics

The moist QG system has dynamics which extend beyond the range of its unstable modes. Held and Larichev (1996) argue that the energetic of the (dry) QG system can be decomposed between an inverse energy cascade associated with barotropic motions, and a direct cascade of available potential energy. The two cascades are coupled in the sense that the available potential energy is gradually converted into kinetic energy as it moves toward smaller scales, which sustains the inverse barotropic kinetic energy cascade. We will now revisit how the inclusion of moist processes modify this picture by providing an additional source of kinetic energy associated with the poleward transport of water vapor.

As in a classical QG system, the energetics can be deconstructed into barotropic and baroclinic components. The barotropic energy is purely a kinetic energy term constructed as $\mathrm{EKE}_B = \left|\nabla\psi_B'\right|^2/2$. Its evolution in the domain average can be constructed from Equation (1) as

$$\partial_t \overline{\mathrm{EKE}}_B = \mathcal{B} - \mathcal{D}_B. \tag{24}$$

The barotropic energy equation is unchanged from the dry QG case. It receives injections of energy from the baroclinic mode ($\mathcal{B} = \overline{\psi_B' J\left(\psi_b' - U/2y, \nabla^2\psi_b'\right)}$) and dissipates via an Ekman term $\mathcal{D}_B = \overline{r\nabla\psi_B' \cdot \nabla\left(\psi_B' - \psi_b'\right)}/2$. Here, the overline indicates a domain average. Additional interactions between the two modes can arise from the Ekman term via correlations between the barotropic and baroclinic velocity; however, this will be disregarded in the considerations here.

The baroclinic energy consists of a kinetic energy component $\mathrm{EKE}_b = \left|\nabla\psi_b'\right|^2/2$ and an available potential energy component APE$= g^*\eta'^2/4H$. In the domain average, its evolution can be computed from the baroclinic potential vorticity as

$$\partial_t \overline{E_b} = -\mathcal{B} - \mathcal{D}_b + \epsilon_{APE} + \mathcal{P}. \tag{25}$$

The baroclinic energy equation is also quite similar to its dry counterpart. The first term is the transfer from the baroclinic to the barotropic mode as described above, and the Ekman term $\mathcal{D}_b = \overline{r\nabla\psi'_b \cdot \nabla\left(\psi'_B - \psi'_b\right)}/2$ dissipates kinetic energy, similar to the corresponding term in the barotropic equation. The APE is generated by a downgradient flux of sensible heat $\epsilon_{APE} = -g^*\overline{\eta}_y\overline{v'_B\eta'}/2H$ that acts as a source of baroclinic energy at small scales. The sole modification from moisture is the additional source represented by the final term, $\mathcal{P} = g^*\mathcal{L}\overline{P'\eta'}/2H$. This characterizes the generation of APE due to the injection of latent heat.

a. Moist Energy

The impact of moisture depends on the amount of energy generated from precipitation, and therefore an estimate for the scaling of the precipitation term is necessary. To do this, we construct a quantity which combines the interface and moisture equation to eliminate the tendency term associated with ageostrophic convergence. This term is then forced only by the diabatic terms, i.e.

$$\frac{D_B}{Dt}\left(\eta + m\right) = J\left(\psi_b, m\right) - \left(1 - \mathcal{L}\right)\left(P - E\right). \tag{26}$$

To interpret this quantity, let us consider an adiabatic adjustment to the interface and moisture, such that the system is then exactly at saturation. Then, the new interface relates to the new moisture content as $\eta_w = Cm_w$. Since $\eta + m$ is conserved in the absence of diabatic forcing, we expect

$$\eta + m = \eta_w + m_w = \left(1 + C\right)\eta_w. \tag{27}$$

The quantity η_w has similarities with the concept of a wet bulb temperature, as defined in e.g. Pauluis et al. (2008). We therefore define it as a wet bulb thickness,

$$\eta_w = \frac{\eta + m}{1 + C} = \eta + \frac{m - m_s}{1 + C}. \tag{28}$$

For a system everywhere at saturation, $\eta_w = \eta$. The evolution of the wet bulb thickness can be expressed as

$$\frac{D_B}{Dt}\eta_w = J(\psi_b, \eta_w) - \frac{\mathcal{L}P}{\mu_s - 1}. \tag{29}$$

From this, we can construct a moist energy (ME) of the form

$$\mathrm{ME} = \frac{g^*}{4H}(\mu_s - 1)\eta_w'^2. \tag{30}$$

In the domain average, the ME evolves as

$$\partial_t \overline{\mathrm{ME}} = \epsilon_{ME} - \mathcal{P} - \mathcal{D}_P. \tag{31}$$

The first term captures the generation of ME, with further elaboration below. The second term of Equation (31) captures the transfer from ME to APE by precipitation. The third captures the dissipation of ME due to precipitation $\mathcal{D}_P = -(g^* H/2)\left[\mathcal{L}/(1+C)\right]\tau\overline{P'^2}$, which vanishes in the limit $\tau \to 0$. This third term will be neglected going forward because of the assumptions of the saturated limit. The generation of ME can be written as

$$\epsilon_{ME} = -\frac{g^*}{2H}(\mu_s - 1)\overline{\eta}_y\overline{\left(v_B' - v_b'\right)\eta_w'}. \tag{32}$$

This captures the role of the downgradient flux of both moisture and thickness in generating the moist energy. In the saturated limit, this reduces nicely to

$$\epsilon_{ME,s} = -\frac{g^*}{2H}(\mu_s - 1)\overline{\eta}_y\overline{v_B'\eta'}. \tag{33}$$

In this limit, the generation of ME is shown to be proportional to the downgradient thickness flux from Equation (25). We can then combine Equation (25) and Equation (31) at saturation to create a budget for the total saturated moist baroclinic energy $E_{mb,s}$,

$$\partial_t \overline{E_{mb,s}} = -\mathcal{B} - \mathcal{D}_b + \epsilon_{APE} + \epsilon_{ME,s}. \tag{34}$$

The total energy generation of the system can then be computed as $\epsilon = \epsilon_{APE} + \epsilon_{ME}$, which at saturation becomes

$$\epsilon_s = \epsilon_{APE} + \epsilon_{ME,s} = -\mu_s \frac{g^*}{2H}\overline{\eta}_y \overline{v'_B \eta'}, \tag{35}$$

with corresponding dissipation

$$\mathcal{D} = \frac{r}{2}\overline{\left|\nabla\left(\psi'_B - \psi'_b\right)\right|^2} \tag{36}$$

The moist energy cycle described here is depicted in Figure 4. The advantage of our description is an isolation of the moist energy ME, which then interacts with a dry system that behaves the same as classical 2-layer QG, except for a forcing associated with precipitation.

b. Scaling of the Energy Tendency Terms

A fundamental assumption in scaling arguments for quasi-geostrophic turbulence is a statistical balance between the generation and the dissipation of energy over long time scales. For the total energy, this predicts

$$\frac{\langle\epsilon\rangle}{\langle\mathcal{D}\rangle} = 1, \tag{37}$$

where the brackets indicate a sufficiently long time average.

We can also test whether individual energy components - notably EKE_b and ME - will reach a statistical equilibrium. Hence we predict,

$$\begin{aligned} \frac{\langle\mathcal{B}\rangle}{\langle\epsilon\rangle} &= 1, \\ \frac{\langle\mathcal{P}\rangle}{\langle\epsilon_{ME}\rangle} &= 1. \end{aligned} \tag{38}$$

Lastly, the saturated limit predicts $\langle\epsilon_{ME}\rangle = (\mu_s - 1)\langle\epsilon_{APE}\rangle$. Hence we also expect to see,

$$\frac{\langle\mathcal{P}\rangle}{\langle\epsilon_{APE}\rangle} = \mu_s - 1. \tag{39}$$

Figure 5 explores the robustness of these scaling relationships in numerical simulations. We can see that the dissipative relationships hold more clearly for smaller injections of energy, with dissipation exceeding the energy generation for more supercritical flow, ultimately leading to an an

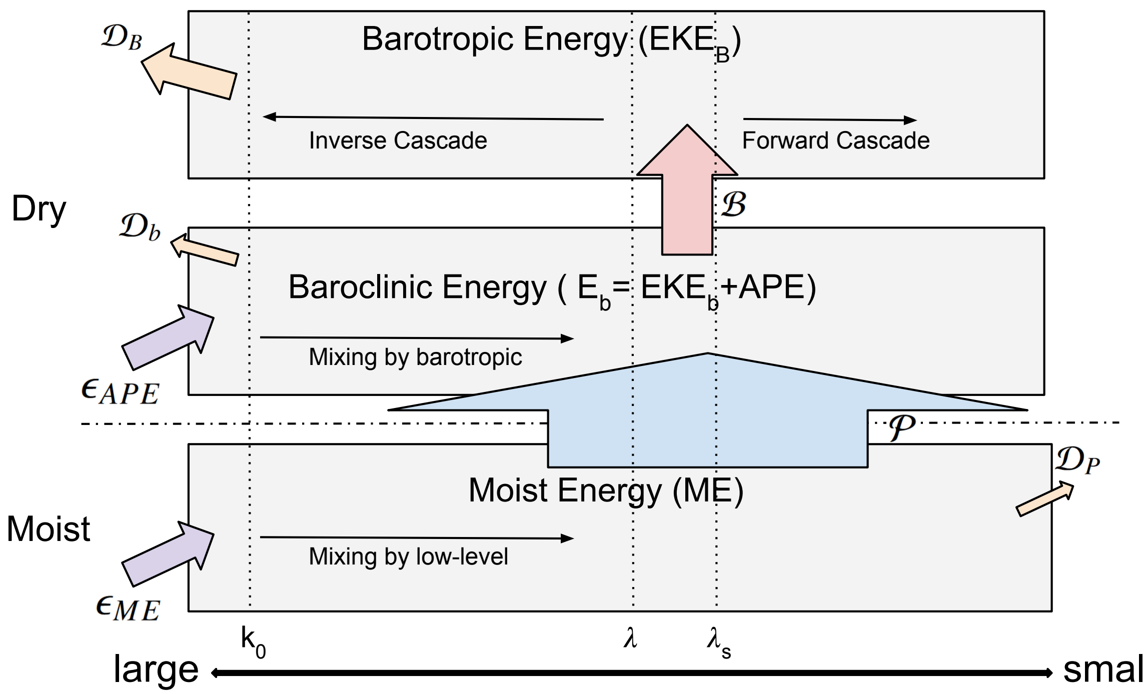

FIG. 4. Energy transfers in the MQG model, with the estimates of the scaling at saturation. At large scales, the background moisture and temperature gradients are redistributed by the barotropic flow, acting as a source for the APE and ME, ϵ_{APE} and ϵ_{ME}, respectively (purple arrows). The energy is mixed to smaller scales by the barotropic flow until near the Rossby radius. The precipitation $\mathcal{P}$ (blue arrow) acts as a broad-spectrum transfer of ME into APE across, with a peak near the saturated Rossby radius. The baroclinic mode injects energy into the barotropic $\mathcal{B}$ (red arrow), predominantly between the dry and saturated Rossby radius. The barotropic flow has an inverse energy cascade to larger scales and a forward enstrophy cascade to smaller scales. Dissipation (orange arrows) occurs primarily through Ekman dissipation of the barotropic mode $\mathcal{D}_B$ at large scales. Additional dissipation occurs with Ekman dissipation of the baroclinic mode $\mathcal{D}_b$ at large scales and precipitation dissipation $\mathcal{D}_P$ mostly at small scales. Additional small-scale dissipation occurs in the barotropic and baroclinic modes, but is not depicted here.

offset of around 20%. It is possible that this is the result of differences in averaging across different simulations. The injection into the barotropic mode $\mathcal{B}$ scales closely with the generation of MAE across all simulations, verifying that $\mathcal{B}$ can be approximated by ϵ. The moist energy exhibits a balance between its generation and loss due to precipitation, robust across all simulations in this saturated regime. The precipitation scales as predicted with the sensible heat flux at small values of

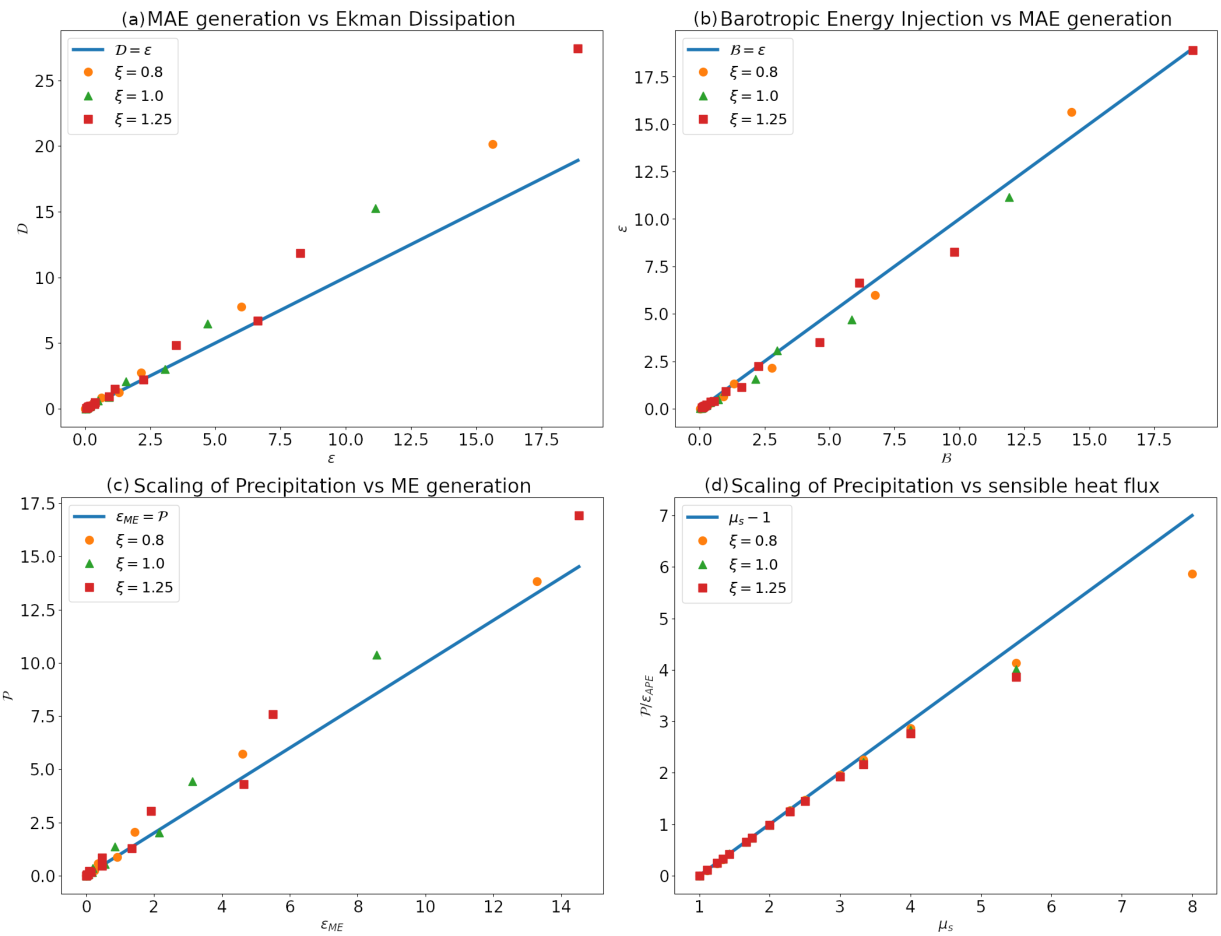

FIG. 5. The predicted balance of (a) the total generation of energy vs the Ekman dissipation, (b) the generation of MAE vs the injection into barotropic energy, (c) the generation of ME and injection to APE by precipitation, and (d) the scaling of the precipitation injection versus the generation of APE by downgradient flux of sensible heat, as $\mu_s - 1$.

μ_s, but becomes less correlated at higher values. However, higher values of μ_s also correlate with more subsaturated points in the simulation, so it is possible that the decrease in energy generated from precipitation corresponds with a lower degree of saturation.

c. Rhines scale and the Inverse Cascade

Linear stability analysis suggests that the spectrum of unstable modes does not expand to larger scales, but does increase in growth rate. We can assess this in the non-linear case by considering a

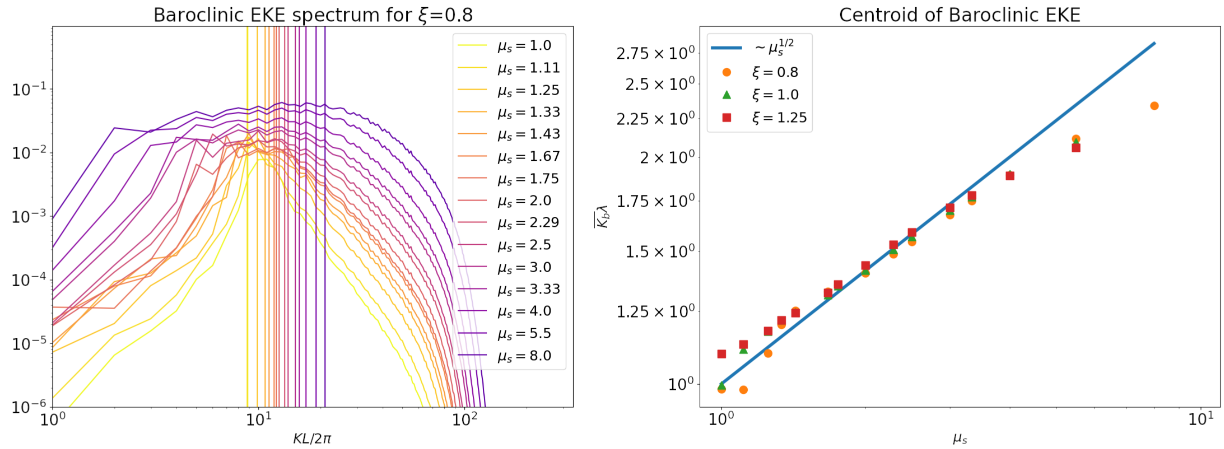

FIG. 6. The baroclinic kinetic energy spectrum with the straight lines depicting the position of the centroid of the corresponding vertical line (left), and the scaling of the centroid with $\mu_s^{1/2}$ (right). For reference, the dry Rossby radius $\lambda = 9KL/2\pi$.

centroid of the baroclinic energy spectrum, defined by

$$\overline{K_b}^2 = \frac{\int K^2 \mathrm{EKE}_b dK}{\int \mathrm{EKE}_b dK}. \tag{40}$$

Figure 6 verifies that the baroclinic energy spectrum exhibits growth on all scales with increasing moist parameters, but more at small scales than large. The centroid of the baroclinic mode shifts to smaller scales as μ_s increases, but does not vary much with the dry criticality.

If the largest injection scale does not change by much, the inverse cascade ought to have the same spectral properties as it would in the dry case. The arguments of Held and Larichev (1996) predict that the termination of the inverse cascade can be estimated by assuming the baroclinic potential vorticity perturbation is mixed downgradient by turbulent diffusion until being reassimilated into the barotropic flow near the Rhines scale k_0^{-1}. The equivalent argument in the MQG system would predict the same with the *moist* baroclinic potential vorticity, allowing for an estimate of the typical size of its eddies,

$$q_m' \approx k_0^{-1} \mu_s U \lambda^{-2}. \tag{41}$$

The injection into kinetic energy from MAE can then be approximated as

$$\epsilon = \mu_s U \lambda^{-2} \overline{v'_B \psi'_b} \approx V k_0^{-1} \mu_s U \lambda^{-2}, \tag{42}$$

where V is the root mean square barotropic velocity. For systems with a sufficient inertial range, a secondary estimate for the energy generation can be made using dimensional analysis,

$$\epsilon \approx V^3 k_0. \tag{43}$$

Lastly, the Rhines scale itself can be calculated using the root mean square barotropic velocity,

$$k_0^{-2} = V/\beta. \tag{44}$$

Combined, these provide the following estimates:

$$(k_0 \lambda)^{-1} \approx \mu_s^{1/2} \xi \tag{45}$$

$$\frac{V}{U} \approx \mu_s \xi \tag{46}$$

$$\frac{\epsilon}{U^3 \lambda^{-1}} \approx \mu_s^{5/2} \xi^2 \tag{47}$$

Figure 7a confirms an extension of the inverse cascade as μ_s increases. When $\mu_s = 1.0$, corresponding to a dry atmosphere, the system is subcritical, and thereby does not exhibit an inverse cascade. The corresponding Rhines scale does not capture the termination of the cascade. Similarly, when $\mu_s = 1.33$ and 1.75, the system is weakly supercritical and does not generate enough energy for an inverse cascade, and thereby predicts Rhines scales smaller than the dry Rossby radius $\lambda = 9KL/2\pi$. As the values of μ_s increase, the Rhines scale as predicted by Equation (44) shifts to larger scales as the inverse cascade extends. The $-5/3$ slope of this cascade is not as clear in these models; however, this can be attributed to the relative size of the domain. The forward cascade with a -3 slope is more clear, with an increase in energy at smaller scales as μ_s increases.

Additional perspectives on the scale shift associated with both ξ and μ_s can be seen in Figure 7b-d. The data better aligns with the prediction in the asymptotic limit, as $\xi_s \to \infty$. This limit occurs towards the right of the x-axis on each plot. As expected, the data converges to the predicted slope in as the value of the moist criticality increases. This convergence is most clear in the scaling of

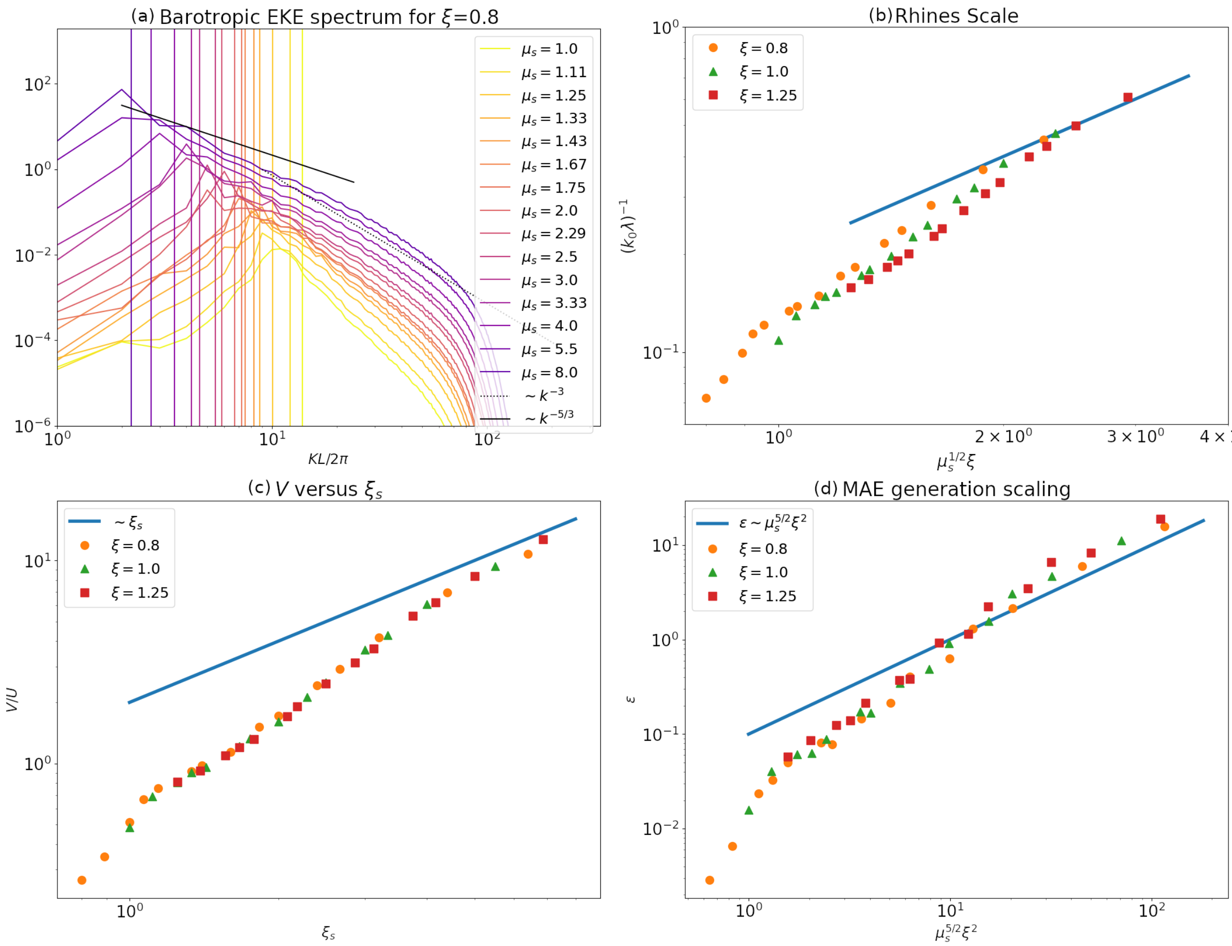

FIG. 7. (a) The barotropic kinetic energy cascades with the Rhines scale as predicted by the RMS barotropic velocity corresponding to the vertical lines, (b) the scaling of the Rhines scale k_0 computed from the RMS barotropic velocity as a function of saturated criticality, (c) the scaling of the RMS barotropic velocity V as a function of saturated criticality $\mu_s\xi$ and (d) the scaling of the total energy generated by the MQG system.

the total energy generation, where the data begins to converge around $\mu_s^{5/2}\xi^2 = 1.0$. The Rhines scale begins to converge around $\mu_s^{1/2}\xi = 2.0$, while the velocity does not reach a clear convergence. It is plausible that in the asymptotic limit, the results would converge to the predictions.

d. Interpreting the Parameter μ_s

The parameter $\mu_s = (1 + C\mathcal{L})/(1-\mathcal{L})$ plays a central role in the MQG system. It shows up in the expression for the saturated moist potential vorticity (14) and in the generation of MAE (35) at saturation. In both occurences, it characterizes a reduction to the effective stratification of the atmosphere as a result of precipitation (Neelin and Held 1987; Emanuel et al. 1994). The larger μ_s is, the lower the effective stratification. A connection between Equation (29) and the wet bulb temperature equation of Pauluis et al. (2008) can be achieved by taking $1-\mu_s^{-1}$ to be the moisture stratification of the system. Similarly, the moist energy of Smith and Stechmann (2017) contains a coefficient defined by vertical gradients of the background moisture content, potential temperature, and equivalent potential temperature that serves a similar role to the $\mu_s - 1$ term that appears in Equation (30).

For a physical insight on how moisture affects both potential vorticity and available energy, let us return to the concept of the effective thickness (12). At saturation, its pertubation equation can be expressed as

$$\frac{D_B}{Dt}\eta' = -\frac{(\overline{\eta}+\mathcal{L}\overline{m})_y}{1+C\mathcal{L}}v_B' - \mu_s^{-1}W. \tag{48}$$

This has two components: the first a downgradient flux of the background effective thickness gradient by the barotropic flow, and the second vertical motion that corrects for local anomalies in the moist thickness. The latter lends itself to a first interpretation of μ_s as the factor by which the vertical motion must increase in the saturated case compared to the dry case in order to correct for a thickness perturbation of the same size. Increasing the parameter C means that precipitation is favored after an upward shift in the interface, counteracting the effect of the vertical motion in correcting for displacements.

The moist available energy (MAE) at saturation can then be constructed up to a constant of proportionality by multiplying the above by $\mu_s\eta'$, yielding

$$\frac{D_B}{Dt}\left(\mu_s\overline{\eta'^2}/2\right) = -\frac{(\overline{\eta}+\mathcal{L}\overline{m})_y}{1-\mathcal{L}}\overline{v_B'\eta'} - \overline{W\eta'}. \tag{49}$$

In this version of the MAE, μ_s appears in the thickness flux term if $\overline{m} = C\overline{\eta}$. This points to a second mechanism by which μ_s predicts an adjustment to the effective static stability, resulting from the meridional redistribution of the background gradient. A larger C acts to generate larger anomalies in the displacement of the effective thickness as a result of the large-scale moisture gradient.

Let us consider a breakdown of μ_s:

$$\mu_s = \underbrace{\frac{1}{1-\mathcal{L}}}_{\substack{\text{Fractional reduction}\\ \text{in effective static stability}}} + \underbrace{\frac{C\mathcal{L}}{1-\mathcal{L}}}_{\substack{\text{Total effect of correlation}\\ \text{between temperature and moisture}}} . \tag{50}$$

The decrease in effective stratification associated with moisture can here be associated with two processes:

1. The presence of latent heat release over the entire domain of typical scale $\mathcal{L}$, characterized by the first term on the right-hand side of Equation (50). This neglects any dependency of the saturation value on temperature, but takes into account that the presence of latent heat release will result in a compounding effect on the static stability. It can also be written as,

$$\frac{1}{1-\mathcal{L}} = \frac{c_p\delta\theta}{c_p\delta\theta - Lm_0}, \tag{51}$$

   where $c_p\delta\theta$ is the typical cooling of a dry ascending parcel, and $c_p\delta\theta - Lm_0$ is the typical net cooling of a moist ascending parcel.

2. The interactions between moisture and temperature on both local and global scales, characterized by the third term on the right-hand side of Equation (50). On a local scale, a non-zero C favors precipitation in response to upward vertical motion, which counteracts the effect of said motion. On a global scale, the background moisture content gradient scales as C. The downgradient transport of effective thickness results in surplus moisture relative to a colder environment, and thus additional latent heat is released. This term vanishes if we neglect any correlation between the saturation moisture and temperature.

5. Conclusion

We have investigated the scaling of an idealized MQG system analogous to the one described in Lapeyre and Held (2004) with a deconstruction into barotropic and baroclinic modes. This system features moisture and latent heat release as an additional source of available energy, calling for an updated understanding of the energetics and conserved quantities of the system. We provided an updated framework for the energy that describes a transition of energy from (1) downgradient fluxes of temperature and moisture to (2) moist energy to (3) available potential energy and finally (4) kinetic energy. Associated with this new framework is a moist baroclinic potential vorticity which is conserved under latent heat release. This modified potential vorticity emphasizes a gradient that takes into account the background meridional configuration of both temperature and moisture.

An interesting limit occurs when the atmosphere is saturated everywhere, which can be achieved by enforcing a high rate of evaporation and a fast relaxation time for precipitation. Under this limit, the MQG system is mathematically equivalent to the dry two-layer QG equations after rescaling both the time and spatial scales. In particular, this saturated limit makes it possible to extend previous results from geostrophic turbulence to include the effect of moisture on the dynamics of baroclinic eddies. In conjunction with this, we introduced a saturated criticality, the dry criticality rescaled by a parameter μ_s, which predicts instability under configurations where the dry case would predict stability.

First, we analyzed the conditions for baroclinic instability in the saturated limit using a linear stability analysis. A dry system predicts instability when the mean baroclinic potential vorticity gradient is larger than the gradient of the Coriolis parameter. The analysis presented here predicts instability when the mean *moist* baroclinic potential vorticity gradient is larger than the gradient of the Coriolis parameter. Depending on the interpretation, we can see this either as updating the thermodynamic gradient for instability analysis from temperature to a combination of temperature and moisture; or as modifying the static stability of the system to reflect the additional vertical instability generated by latent heat release. In practice, it might be more helpful to imagine a combination of the two associated with the diagonal propagation of motion poleward and upward, both of which result in air parcels being transported to a colder and drier environment, which can trigger dry baroclinic instability, latent heat release, or both. We confirm numerically that the fully non-linear MQG system exhibits instability at smaller scales and an increase in the total energy injection. This provides additional supporting evidence that the increase in the intensity of moist storms requires the resolution of sufficiently small spatial scales, as shown in, e.g., Booth et al. (2013); Willison et al. (2015).

We introduced an energetic framework that characterizes of the injection of moist energy into available potential energy via precipitation. From an energetic point of view, the large-scale moisture gradient acts as a reservoir of moist energy. Eddies extract moist energy by transporting moisture poleward, which is then converted to available potential energy when precipitation occurs in the warm sector of the eddies. This provides an additional source of baroclinic energy, which can significantly energize moist geostrophic turbulence when compared to its dry counterpart under the same temperature gradient. We verified numerically that this modified energetic framework exhibits the long-term statistical balances expected of a turbulent system.

This increase in the generation of eddy kinetic energy in presence of a moisture gradient enhances the inverse cascade of barotropic kinetic energy, similar to the arguments presented in Held and Larichev (1996). In particular, the Rhines scale associated with the end of the inverse cascade shifts to larger scale in presence of a moisture gradient. We confirmed this numerically by calculating the Rhines scale from the RMS barotropic velocity.

The energetic framework described here is mathematically equivalent to the framework introduced in Lapeyre and Held (2004), albeit with different choices in which terms to include and exclude. However, the philosophical approach between the two constructions differs. Where theirs is based upon the evolution of the moist static energy and the moisture deficit or surplus, ours separates the dry and moist energy terms by constructing an analogue to wet bulb temperature, which evolves with diabatic forcing only. This allows for a clear cycle of energy generation, transfers between different terms, and dissipation. This formulation of moist energy more closely resembles that of some tropical models such as Pauluis et al. (2008); Frierson et al. (2004). Likewise, the moist energy formulation of Smith and Stechmann (2017) can be reworked into a quadratic of a quantity similar to the wet bulb temperature, proportional to the dry potential temperature of a system brought adiabatically to saturation. More work is needed to bridge the gap between the energetics of these idealized models and other models of moist atmospheric dynamics, such as a continuously stratified system. Based on the results here, it is worth exploring whether a Moist Energy can be constructed based on the wet bulb temperature or lifting condensation level.

The revised criticality parameter associated with the saturated system suggests a reinterpretation of classic baroclinic adjustment arguments such as in Stone (1978). The dry criticality of the earth's atmosphere is predicted to remain around $\xi \approx 1$ across different climate simulations. However, if instead instability is set by an effective moist criticality, the assumptions underlying this adjustment are changed. Let us return to the thought experiment of a planet warming uniformly at the surface for insight. We can estimate an increase in the moisture availability by 7% per K, translating to a comparable increase in the gradient. Naively, one could start by simply increasing parameter μ_S, leaving the temperature gradient fixed (i.e., fixed dry criticality ξ). This will lead to greater instability and more energy transport poleward, as observed in the difference between the integrations in the top two rows in Figure 2 (here a very large change in moisture was forced to emphasize the differences).

The increase in meridional heat transport, however, would demand a change in the energy balance at the top of the atmosphere. If we instead assume that the top of the atmosphere balance remains about the same, then the meridional transport of energy is fixed. Warming the planet will increase the moisture gradient, hence the temperature gradient must decrease. If the transport scales with the total criticality $\xi_s = \mu_s \xi$, then the dry criticality must decrease to compensate for the increase in the moisture gradient. How does this new world, with the more moisture, but the same total criticality, compare to the original one? If an effective moist criticality is conserved, this study predicts smaller scale motion associated with a larger generation of Moist Available Energy, as seen in the comparison between the integrations in the second and third rows of Figure 2.

There are a few areas where further research could help clarify the results of this study and its implications on the atmosphere. Data-driven studies could provide a better estimate of the relative change in static stability and latent heat release across different climates. Warming predicts both an increase in both the dry static stability and the moisture content (Frierson et al. 2006). As a result, both the numerator and the denominator of $\mathcal{L}$ are expected to increase. The question of which change will dominate on a global scale depends on a number of factors, including the amount and distribution of rainfall.

Another natural follow-up is the case of partial saturation, which introduces additional complications to the moist system. A stability analysis based on the full energetics of the system would be necessary to predict the changes to the effective moist criticality. Furthermore, the decorrelation of moisture from temperature adds an additional degree of freedom, requiring a full consideration of the corresponding terms in the energy and moist potential vorticity that were neglected here. Open questions remain about how the partially saturated system will exhibit instability: perhaps the water content, being advected by both the larger scale barotropic flow and the smaller scale baroclinic flow, will exhibit persistent features on smaller scales than the temperature, allowing for instabilities at smaller scales that predicted in either the dry or saturated case. The energetic framework provided here can be used to analyse these additional terms and determine the changes to scalings associated with them.

Acknowledgments. Thanks to Shafer Smith for guidance on implementing the QG model. MLB and EPG acknowledge support from the US National Science Foundation through award AGS-1852727. MLB and OP acknowledge support by the National Science Foundation under Grant HDR-1940145 and by the New York University in Abu Dhabi Research Institute under Grant G1102.

Data availability statement. The code used to generate the data in this study is stored in the repository at `https://github.com/margueriti/Moist_QG_public`.

APPENDIX A

Precipitation Closure

We use the closure described in Lapeyre and Held (2004), based on the idea of conservation of effective thickness in the domain average:

$$\partial_t \left(\overline{\eta + \mathcal{L}m}\right) = 0. \tag{A1}$$

Hence if we pick an initial value $\overline{\eta + \mathcal{L}m} = 0$, we can expect this quantity to be conserved over time. These domain averages then evolve with the precipitation and evaporation as

$$\begin{aligned} \partial_t \overline{m} &= \overline{E - P} \\ \partial_t \overline{\eta} &= \mathcal{L}\left(\overline{P - E}\right). \end{aligned} \tag{A2}$$

Hence the total precipitation can be expressed as

$$P = \begin{cases} \left[(1 + C\mathcal{L})\,\overline{m} + m' - C\eta'\right]/\tau & \text{where } m > m_s \\ 0 & \text{where } m \le m_s \end{cases}. \tag{A3}$$

APPENDIX B

Equivalence of Dry and Saturated Limits

We introduce some rescalings to nondimensionalize:

$$(x,y) \to \lambda^{-1}(x,y) \tag{B1}$$
$$t \to U\lambda^{-1}t \tag{B2}$$
$$\beta \to U^{-1}\lambda^{2}\beta \tag{B3}$$
$$r \to U^{-1}\lambda r \tag{B4}$$
$$\psi \to U^{-1}\lambda^{-1}\psi \tag{B5}$$
$$q \to U^{-1}\lambda q \tag{B6}$$
$$\eta \to U^{-1}\lambda f_0\eta \tag{B7}$$
$$W \to U^{-2}\lambda^{2} f_0\frac{W}{H} \tag{B8}$$
$$m \to U^{-1}\lambda f_0 m/H \tag{B9}$$
$$P \to U^{-2}\lambda^{2} f_0 P/H, \tag{B10}$$

with λ and U, respectively the reference length and velocity scales, rescaled as the unit. The resulting perturbation equations can then be written as

$$\frac{D_B q'_B}{Dt} = -J\left(\psi'_b, q'_b\right) - \frac{1}{2}\partial_x\nabla^2\psi'_b - \beta\partial_x\psi'_B - \frac{r}{2}\nabla^2\psi'_2 \tag{B11}$$
$$\frac{D_B q'_b}{Dt} = -J\left(\psi'_b, q'_B\right) - \frac{1}{2}\partial_x q'_B - \beta\partial_x\psi'_b - \partial_x\psi'_B + \frac{r}{2}\nabla^2\psi'_2 - \mathcal{L}P' \tag{B12}$$
$$\frac{D_B \eta'}{Dt} = v'_B - W + \mathcal{L}P' \tag{B13}$$
$$\frac{D_B m'}{Dt} = +J\left(\psi'_b, m'\right) + \frac{1}{2}\partial_x m' + C\left(v'_B - v'_b\right) - P' + W \tag{B14}$$
$$\frac{D_B q'_m}{Dt} = -J\left(\psi'_b, q'_B - \frac{\mathcal{L}}{1-\mathcal{L}}m'\right) - \frac{1}{2}\partial_x q'_B - \beta\partial_x\psi'_b - \mu_s v'_B + \frac{1}{2}\frac{\mathcal{L}}{1-\mathcal{L}}\partial_x\left(m' - m'_s\right) + \frac{r}{2}\nabla^2\psi'_2, \tag{B15}$$

where the operator D_B/Dt denotes advection by the barotropic flow. In an atmosphere that is everywhere at saturation, the moist baroclinic potential vorticity becomes

$$q'_m = \nabla^2\psi'_b - 2\mu_s\lambda^{-2}\psi'_b, \tag{B16}$$

with governing equation

$$\frac{D_B q_m'}{Dt} = -J\left(\psi_b', q_B'\right) - \frac{1}{2}\partial_x q_B' - \beta\partial_x\psi_b' - \frac{1+C\mathcal{L}}{1-\mathcal{L}}\partial_x\psi_B' + \frac{r}{2}\nabla^2\psi_2', \tag{B17}$$

which closely resembles the baroclinic mode except for one term with a factor of $\mu_s = \frac{1+C\mathcal{L}}{1-\mathcal{L}}$. If we instead scale the length by $\lambda_s = \mu_s^{-1/2}\lambda$ and substitute accordingly in all other rescalings, the governing equation for moist baroclinic potential vorticity at saturation then becomes

$$\partial_t q_m' + J\left(\psi_B', q_m'\right) + J\left(\psi_b', q_B'\right) = -\frac{1}{2}\partial_x q_B' - \beta\partial_x\psi_b' - \partial_x\psi_B' + \frac{r}{2}\nabla^2\psi_2'. \tag{B18}$$

Noting that $J\left(\psi_b', q_b'\right) = J\left(\psi_b', \nabla^2\psi_b'\right) = J\left(\psi_b', \tilde{q}_m'\right)\big|_{sat}$, the barotropic mode is unchanged under the rescaling and can be thought of as forced by the moist baroclinic mode. Hence we have a closed pair of governing equations identical to the governing equations for the dry two-layer baroclinic instability, and so the saturated limit is equivalent to the dry case with a rescaling.

References

Betts, A. K., and M. J. Miller, 1986: A new convective adjustment scheme. Part II: Single column tests using GATE wave, BOMEX, ATEX and arctic air-mass data sets. *Quarterly Journal of the Royal Meteorological Society*, **112 (473)**, 693–709, https://doi.org/10.1002/qj.49711247308, URL https://rmets.onlinelibrary.wiley.com/doi/abs/10.1002/qj.49711247308.

Booth, J. F., S. Wang, and L. Polvani, 2013: Midlatitude storms in a moister world: lessons from idealized baroclinic life cycle experiments. *Climate Dynamics*, **41 (3)**, 787–802, https://doi.org/10.1007/s00382-012-1472-3, URL https://doi.org/10.1007/s00382-012-1472-3.

Bretherton, C. S., M. E. Peters, and L. E. Back, 2004: Relationships between Water Vapor Path and Precipitation over the Tropical Oceans. *Journal of Climate*, **17 (7)**, 1517–1528, https://doi.org/10.1175/1520-0442(2004)017<1517:RBWVPA>2.0.CO;2, URL https://journals.ametsoc.org/view/journals/clim/17/7/1520-0442_2004_017_1517_rbwvpa_2.0.co_2.xml.

Edwards, T. K., L. M. Smith, and S. N. Stechmann, 2019: Spectra of atmospheric water in precipitating quasi-geostrophic turbulence. *Geophysical & Astrophysical Fluid Dynamics*, **0 (0)**, 1–27, https://doi.org/10.1080/03091929.2019.1692205, URL https://doi.org/10.1080/03091929.2019.1692205.

Emanuel, K. A., M. Fantini, and A. J. Thorpe, 1987: Baroclinic Instability in an Environment of Small Stability to Slantwise Moist Convection. Part I: Two-Dimensional Models. *Journal of the Atmospheric Sciences*, **44 (12)**, 1559–1573, https://doi.org/10.1175/1520-0469(1987)044<1559:BIIAEO>2.0.CO;2, URL https://journals.ametsoc.org/jas/article/44/12/1559/21713/Baroclinic-Instability-in-an-Environment-of-Small.

Emanuel, K. A., J. D. Neelin, and C. S. Bretherton, 1994: On large-scale circulations in convecting atmospheres. *Quarterly Journal of the Royal Meteorological Society*, **120 (519)**, 1111–1143, https://doi.org/10.1002/qj.49712051902, URL https://rmets.onlinelibrary.wiley.com/doi/abs/10.1002/qj.49712051902.

Frierson, D. M. W., I. M. Held, and P. Zurita-Gotor, 2006: A Gray-Radiation Aquaplanet Moist GCM. Part I: Static Stability and Eddy Scale. *Journal of Atmospheric Sciences*, **63 (10)**, 2548–2566, https://doi.org/10.1175/JAS3753.1, URL https://journals.ametsoc.org/view/journals/atsc/63/10/jas3753.1.xml.

Frierson, D. M. W., A. J. Majda, and O. M. Pauluis, 2004: Large Scale Dynamics of Precipitation Fronts in the Tropical Atmosphere: A Novel Relaxation Limit. *Communications in Mathematical Sciences*, **2 (4)**, 591–626, URL https://projecteuclid.org/euclid.cms/1109885499.

Held, I. M., and V. D. Larichev, 1996: A Scaling Theory for Horizontally Homogeneous, Baroclinically Unstable Flow on a Beta Plane. *Journal of the Atmospheric Sciences*, **53 (7)**, 946–952, https://doi.org/10.1175/1520-0469(1996)053<0946:ASTFHH>2.0.CO;2, URL https://journals.ametsoc.org/jas/article/53/7/946/24256/A-Scaling-Theory-for-Horizontally-Homogeneous.

Lambaerts, J., G. Lapeyre, and V. Zeitlin, 2011a: Moist versus Dry Barotropic Instability in a Shallow-Water Model of the Atmosphere with Moist Convection. *Journal of the Atmospheric Sciences*, **68 (6)**, 1234–1252, https://doi.org/10.1175/2011JAS3540.1, URL https://journals.ametsoc.org/jas/article/68/6/1234/27200/Moist-versus-Dry-Barotropic-Instability-in-a.

Lambaerts, J., G. Lapeyre, and V. Zeitlin, 2012: Moist versus Dry Baroclinic Instability in a Simplified Two-Layer Atmospheric Model with Condensation and

Latent Heat Release. *Journal of the Atmospheric Sciences*, **69 (4)**, 1405–1426, https://doi.org/10.1175/JAS-D-11-0205.1, URL https://journals.ametsoc.org/jas/article/69/4/1405/27320/Moist-versus-Dry-Baroclinic-Instability-in-a.

Lambaerts, J., G. Lapeyre, V. Zeitlin, and F. Bouchut, 2011b: Simplified two-layer models of precipitating atmosphere and their properties. *Physics of Fluids*, **23 (4)**, 046 603, https://doi.org/10.1063/1.3582356, URL https://aip.scitation.org/doi/10.1063/1.3582356.

Lapeyre, G., and I. M. Held, 2004: The Role of Moisture in the Dynamics and Energetics of Turbulent Baroclinic Eddies. *Journal of the Atmospheric Sciences*, **61 (14)**, 1693–1710, https://doi.org/10.1175/1520-0469(2004)061<1693:TROMIT>2.0.CO;2, URL https://journals.ametsoc.org/jas/article/61/14/1693/25579/The-Role-of-Moisture-in-the-Dynamics-and.

Lorenz, E. N., 1978: Available energy and the maintenance of a moist circulation. *Tellus*, **30 (1)**, 15–31, https://doi.org/10.1111/j.2153-3490.1978.tb00815.x, URL https://onlinelibrary.wiley.com/doi/abs/10.1111/j.2153-3490.1978.tb00815.x.

Neelin, J. D., and I. M. Held, 1987: Modeling Tropical Convergence Based on the Moist Static Energy Budget. *Monthly Weather Review*, **115 (1)**, 3–12, https://doi.org/10.1175/1520-0493(1987)115<0003:MTCBOT>2.0.CO;2, URL https://journals.ametsoc.org/view/journals/mwre/115/1/1520-0493_1987_115_0003_mtcbot_2_0_co_2.xml.

Pauluis, O., A. Czaja, and R. Korty, 2010: The Global Atmospheric Circulation in Moist Isentropic Coordinates. *Journal of Climate*, **23 (11)**, 3077–3093, https://doi.org/10.1175/2009JCLI2789.1, URL https://journals.ametsoc.org/view/journals/clim/23/11/2009jcli2789.1.xml.

Pauluis, O., D. M. W. Frierson, and A. J. Majda, 2008: Precipitation fronts and the reflection and transmission of tropical disturbances. *Quarterly Journal of the Royal Meteorological Society*, **134 (633)**, 913–930, https://doi.org/10.1002/qj.250, URL https://onlinelibrary.wiley.com/doi/10.1002/qj.250.

Schneider, T., and P. A. O'Gorman, 2008: Moist Convection and the Thermal Stratification of the Extratropical Troposphere. *Journal of the Atmospheric Sciences*, **65 (11)**, 3571–3583, https://doi.org/10.1175/2008JAS2652.1, URL https://journals.ametsoc.org/jas/article/65/11/3571/16887/Moist-Convection-and-the-Thermal-Stratification-of.

Shaw, T. A., and Coauthors, 2016: Storm track processes and the opposing influences of climate change. *Nature Geoscience*, **9 (9)**, 656–664, https://doi.org/10.1038/ngeo2783, URL https://www.nature.com/articles/ngeo2783.

Smith, L. M., and S. N. Stechmann, 2017: Precipitating Quasigeostrophic Equations and Potential Vorticity Inversion with Phase Changes. *Journal of the Atmospheric Sciences*, **74 (10)**, 3285–3303, https://doi.org/10.1175/JAS-D-17-0023.1, URL https://journals.ametsoc.org/jas/article/74/10/3285/216198/Precipitating-Quasigeostrophic-Equations-and.

Stone, P. H., 1978: Baroclinic Adjustment. *Journal of the Atmospheric Sciences*, **35 (4)**, 561–571, https://doi.org/10.1175/1520-0469(1978)035<0561:BA>2.0.CO;2, URL https://journals.ametsoc.org/view/journals/atsc/35/4/1520-0469_1978_035_0561_ba_2_0_co_2.xml.

Vallis, G. K., 2006: *Atmospheric and oceanic fluid dynamics: fundamentals and large-scale circulation*. Cambridge University Press, Cambridge, oCLC: ocm70671784.

Willison, J., W. A. Robinson, and G. M. Lackmann, 2015: North Atlantic Storm-Track Sensitivity to Warming Increases with Model Resolution. *Journal of Climate*, **28 (11)**, 4513–4524, https://doi.org/10.1175/JCLI-D-14-00715.1, URL https://journals.ametsoc.org/view/journals/clim/28/11/jcli-d-14-00715.1.xml.

Wu, Y., and O. Pauluis, 2014: Midlatitude Tropopause and Low-Level Moisture. *Journal of Atmospheric Sciences*, **71 (3)**, 1187–1200, https://doi.org/10.1175/JAS-D-13-0154.1, URL https://journals.ametsoc.org/view/journals/atsc/71/3/jas-d-13-0154.1.xml.